RSC Advances

Reduced Graphene Oxide/Nano-Bioglass Composites: Processing and Super-Anion Oxide Evaluation

Journal:	*RSC Advances*
Manuscript ID	RA-COM-12-2015-027160.R1
Article Type:	Communication
Date Submitted by the Author:	05-Feb-2016

Complete List of Authors:	Chandrasekar, ASHOK RAJA; University of Madras, National Centre for Nanoscience and Nanotechnology Subramanian, BALAKUMAR; UNIVERSITY OF MADRAS, NATIONAL CENTRE FOR NANOSCIENCE AND NANOTECHNOLOGY D, Durgalakshmi; University of Madras, National Centre for Nanoscience and Nanotechnology George, Rani; Indira Gandhi Centre for Atomic Research (IGCAR), Corrosion Science and Technology Group Balakrishnan, Anandkumar; Indira Gandhi Centre for Atomic Research (IGCAR), Corrosion Science and Technology Group; U. Kamachi, Mudali; Indira Gandhi Centre for Atomic Research, Corrosion Science & Technology Section - Reprocessing Plant Materials

Subject area & keyword:	Carbon nanomaterials < Nanoscience

Journal Name

COMMUNICATION

Reduced Graphene Oxide/Nano-Bioglass Composites: Processing and Super-Anion Oxide Evaluation

Received 00th January 20xx,
Accepted 00th January 20xx

DOI: 10.1039/x0xx00000x

www.rsc.org/

Ashokraja ,[a] S. Balakumar,[a*] D. Durgalakshmi,[a] Rani P. George,[b] B. Anand Kumar[b] and U. Kamatchi Mudali[b]

45S5 Bioglass with mean particle size in nano regime were synthesized and fabricated with rGO sheets using three different strategies. The fabricated nanocomposites were analysed for their bond formations and defects. Morphology, size and distribution of n-BG particles on rGO were visualised. An attempt to understand the super oxide anion production by n-BG particles, rGO and its nanocomposites were studied.

45S5 Bioglass (BG) is one of the prime inventions in the class of bioactive ceramics. In which, it is the only available artificial material which is able to chemically bond with bone swiftly than any other know bioactive ceramics.[1,2] Many researchers have modified the preparation methods, incorporated organic, inorganic materials and functionalize them with biological materials to achieve a compatible implant with the host system. Ideal biomaterials should also able to resist infection, corrosion and must have low mechanical stress, out of these; infection is the first reason for a biomaterial rejection *in vivo*. Researchers now design the biomaterials with variety of antibacterial agents such as; drugs, metal ions, metal and metal oxide nanoparticles and so on.[3-6] Although the exact mechanism for antibacterial activity by nanoparticles is still not clearly understood. The current studies suggest that, Reactive Oxygen Species (ROS) which primarily targets oxygen dependent infectious agents causing deleterious effects. Super-oxide anion is relatively toxic type of ROS naturally deployed by our immune cells to destroy the invading pathogens. It is also well-known that nanoparticles produce enormous ROS.[7] For this reason; one should look into synergetic materials for biomaterial implants. In this scenario, the family of bioactive ceramics including BG has passed through a series of evolution in terms of its chemistry, morphology, formulations, and biocompatibility. Similarly graphene, a member of carbon family is another versatile material conquering the world of research and development with its unique and diversified properties, there are many reports on emphasizing its thermal, mechanical, electrical and other physical properties. But recent reports also show graphene as a potent antibacterial agent and as an inducer in promoting oeteoblast division for ostiffication.[8] Graphene is not a new member of hybrid BG. Powal H.*et al* has investigated the processing bioactivity of 45S5 Bioglass-graphene and Cao G. *et al* have reported the enhancement of its mechanical and biological performance.[9,10] Adding to this, there are many reports on graphene oxide (GO)/hydroxyapatite and reduced graphene oxide (rGO)/hydroxyapatite.[11-13] The advantage of rGO over pristine graphene is, rGO possesses carboxylic acid groups in their edges and epoxy groups in their basal structure where nano-Bioglass (n-BG) can be easily functionalised. Numerous chemical, biological reducing agents and electrochemical methods are available to reduce the graphene oxide in large scale with good quality yield.[14-16] Each reducing agent and reduction process has advantages of its own, our choice resided with hydrazine hydrate for the reason it is more standardized, easy and preferred method of reduction with good quality of rGO. The incorporation of nano sized Bioglass than traditional Bioglass gives enhanced mechanical strength and cell proliferation.[17,18] In the present study we have employed reduced graphene oxide and nano Bioglass as raw materials to fabricate rGO/n-BG nanocomposites which is unprecedented, suggested to improve the mechanical and antibacterial property of Bioglass. Since infection is the major problem in vivo, we have studied in detail on the synthesis strategies of the composites in three different synthesis routes and evaluate the super-oxide anion production studies of the nanocomposites. We have fabricated n-BG particles on rGO sheets in three different methods. The chemicals used in the experiments were purchased from Sigma Aldrich and where of high purity. To start with, n-BG powders are prepared by modified the sol-gel method to yield Bioglass particle in nano regime as reported in our previous literatures.[19] Graphene oxide is prepared by improvised Hummer's method (Tour's method),[20] followed by reduction of graphene oxide using hydrazine hydrate to yield rGO sheets.[21] Then to incorporate n-BG particles over rGO sheets three different strategies were employed. For our understanding the process is named as dispersion, ultrasonication and simultaneous reduction

[a] *National Centre for Nanoscience and Nanotechnology, University of Madras, Guindy Campus, Chennai 600025 India. Fax: 044-22352494/22353309; Tel: 044-22202749; *E-mail: balasuga@yahoo.com*
[b] *Corrosion Science and Technology Division, Materials Characterization Group, Indira Gandhi Centre for Atomic Research, Kalpakkam 603 102, India.*

and explained in brief. During dispersion route fabrication rGO were briefly ultrasonicated for 2 hours during which the layers of rGO sheets were exfoliated. To the sonicated solution, dispersed powders of n-BG was added and stirred for 30 mins, the n-BG particles get functionalised to the epoxy and carboxylic groups in the rGO sheets which yields precipitates of nanocomposites. Similarly for ultrasonication route, rGO suspensions were ultrasonicated for 1h and 30 mins, and then n-BG powders were mixed together and sonicated for another 30 mins. The nanocomposites settle down leaving clear solution on top. For simultaneous reduction, the GO powders were ultrasonicated in water for 2 hours to achieve clear suspension. Later n-BG powders was added to the suspension and stirred for another 30 mins to get GO/n-BG complex. This complex was then reduced using hydrazine hydrate, during which the brown colour suspension become dark black and settles down. The resulting precipitate is the product of rGO/n-BG nanocomposites by simultaneous reduction route. A representation of the fabrication procedures is schematically shown in Fig. 1.

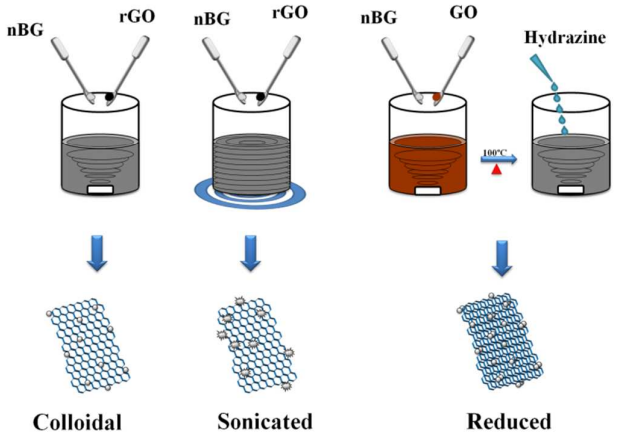

Fig. 1 Schematics showing fabrication of n-BG particles over rGO sheets

The synthesized n-BG powders, rGO and fabricated nanocomposites were studied using Raman, FT-IR, XRD, FESEM and HRTEM to understand the molecular and morphological parameters. A possible evaluation of super-oxide anion radical production was studied by XTT assay using XTT dye (2, 3-bis (2-methoxy-4-nitro-5-sulfophenyl)-2H-tetrazolium-5-carboxanilide).

The bonding nature and vibration modes of silicon-oxygen, phosphates of n-BG particles, D-band and G-band of rGO were analysed for all the samples using Raman and FT-IR spectroscopes, which are complimentary to each other and shown in Fig. 2. The characteristic peaks for different vibrations of Si-O-Si are observed in Raman spectra of n-BG. Generally vibrations of silica networks are observed between 400 cm^{-1} and 1300 cm^{-1}. Rocking vibrations of oxygen atoms moving perpendicular to Si-O-Si plane is observed at 557 cm^{-1} and 625 cm^{-1}. Bending vibration of oxygen from the two adjacent Silica atoms on the Si-O-Si plane are observed at 723 cm^{-1}. Vibrations of non-bridging oxygen atoms and bridging oxygen are observed at 904 cm^{-1} and 1065 cm^{-1} respectively. Symmetric vibrations of Silica ring structures are observed between 800 cm^{-1} and 820 cm^{-1}.Peak observed in the region between 1000 cm^{-1} and 1260 cm^{-1} attributes to the asymmetric vibration of Si-O-Si bridging sequence. Vibrations of phosphates (PO^{-4}) are observed at 573 cm^{-1}, 948 cm^{-1} and 1382 cm^{-1}.[22]

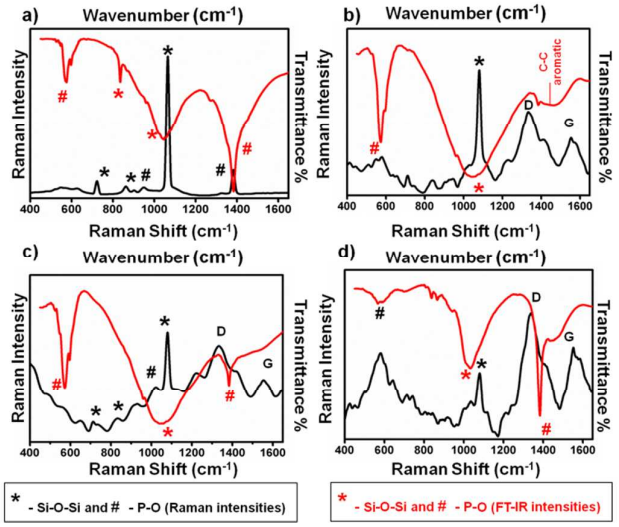

Fig.2 Optical spectroscopy images: FT-IR spectra (red lines) and Raman spectra (black lines of **a)** n-BG, **b)** Dispersion, **c)** Ultra sonicated and **d)** Simultaneously reduced.

The nanocomposites fabricated with n-BG particles and rGO sheets show associated peaks of n-BG and characteristic peaks of rGO. Nanocomposites of rGO/n-BG prepared by different methods exhibit Si-O-Si rocking, bending and bridging oxygen peaks in liaison with pure n-BG samples. Figure in S1 summarises the structural changes of graphite to GO to rGO and the multilayer of rGO sheets. A weak band at 1337 cm^{-1} (D-Band) and a strong band at 1573 cm^{-1} (G-band) in pristine graphite indicate the intact graphitic domains. Following oxidation, the two bands broaden and shift to higher wavenumbers 1374 cm^{-1} and 1598 cm^{-1} with major increase in D-band intensity due to the isolation of carbon double bonds forming GO. After reduction, the D-band intensity decreases slightly with a noticeable increase in G-band, this is attributed to the increase in poly aromatic domains in the defected carbon lattices after reduction. In Fig.2 b), c) and d) raise in D-band intensity is due the oxide groups of silica and other metal oxides in n-BG particles, which undoubtedly specifies the bonding of n-BG particles to the rGO sheets. Similar increase in D-band intensity after grafting of silica nanoparticles and polymers are reported.[23,24] The increment in D-band is higher in ultra sonicated samples than dispersion and reduced samples, also loss of rocking and bending vibrations of Si-O-Si is seen. The reason for such phenomenon could be due to Bioglass bonding to the rGO sheets. Simultaneous reduction of GO/n-BG complex has also resulted in complete loss of bending vibrational peak of Si-O-Si and decrease in bridging oxygen peak, but an increase in rocking vibration is seen. Once again D-band of rGO has dominated all the vibrational peaks.

The FT-IR spectra for n-BG exhibits Si-O-Si peaks centred at 1039 cm^{-1} and at 835 cm^{-1}. [25] As seen in the Fig. 2(a) above, these two peaks are almost complimentary to the Si-O-Si of Raman spectra. Similarly, the peaks centred at 573 attributes to the apatite like calcium phosphate phase of P-O bending[26] and 1384 cm^{-1}attributes to the P-O stretching, C-O and O-H groups in FT-IR is nearly complimentary to Raman spectra.[27] The peaks centred around 1384 cm^{-1}, 1386 cm^{-1} and 1383 cm^{-1} for dispersion, ultra sonicated and simultaneously reduced nanocomposites respectively, corresponds to O-H deformations in C-OH groups of rGO and are also complementary to the D-Band of rGO in Raman spectra.[22] Nanocomposites fabricated by dispersion method did not show much difference in Si-O-Si peaks, but the D-band increased with that of G-band, stating the n-BG particles functionalization with rGO sheets. Whereas, nanocomposites fabricated by ultrasonication method resulted in high particle functionalization on the graphene basal plane, this could be due to the ultra sound waves. Simultaneously reduced GO/n-BG complex did not show any difference in D and G bands, but changes in the Si-O-Si peak centred at 1076 cm^{-1} is observed. This could be due to hydrazine hydrate added to the GO/n-BG complex during reduction process and it could have interacted with the n-BG particles resulting in such changes.

Particles of n-BG and nanocomposites were subjected to XRD analysis to study the sodium calcium silicate systems. Bioglasses are amorphous material, but shows crystalline phases due to the incorporation of sodium to the glass network. 45S Bioglasses prepared by melt quenching method exhibits $Na_2Ca_2Si_3O_9$ crystal system of combite mineral phase, but other phases of sodium calcium silicates are also reported. In our case, we could observe the formation of two mineral phases were identified i.e., sodium calcium silicate (Devitrite) – $Na_2Ca_3Si_6O_{16}$ (JCPDS # 230671) and combite-$Na_4Ca_4Si_6O_{18}$ (JCPDS # 751686), [28,29] as shown in Fig.3.

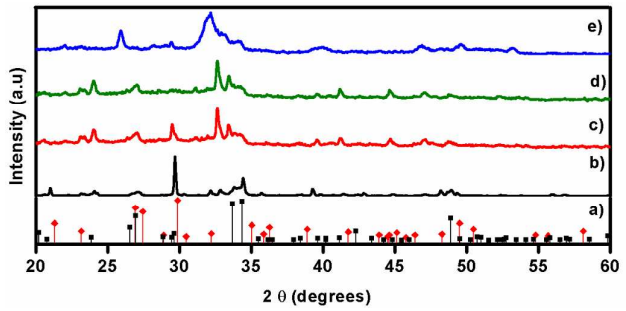

Fig. 3 XRD pattern of nano-Bioglass **b)**, its JCPDS card **a)** – black lines combite and red lines devitrite) and nanocomposites prepared by dispersion method **c)**, ultrasonication **d)** and Simultaneous reduction **e)**

The devitrite phase is not intact to the Bioglass system. Therefore the XRD pattern of nanocomposites exhibited difference in peaks compared to n-BG and its JCPDS standards, which could due to the bonding of rGO sheets to the n-BG particles and depletion of devitrite phase from Bioglass system. Sodium and calcium in silica network acts as network modifiers which are non-covalently bonded. Usually sodium and calcium disassociates from the system under certain conditions, however this has no significant changes in the property of the material. Interestingly in our observation the sodium calcium silicate system of devitrite phase in the composite shows interaction between rGO sheets and n-BG particles has modified the sodium calcium silicate system.[29] In case of nanocomposites prepared by dispersion method, variation in peak intensities was observed. Major peak at 29**°** showed a reduction in intensity, peak centred on 32**°** and 33**°** showed a raise in intensities, which is due to the depletion of devitrite phase and domination of combite phase respectively. Similar changes in sodium calcium silicates were observed in nanocomposites prepared by ultrasonication, but the major peak intensity of devitrite was totally suppressed. Such phenomenon could be due to loss of devitrite phase due to ultrasound waves. Major peak of simultaneously reduced nanocomposites showed peak broadening, which again could be due to the addition of reducing agent. But there was no significant change in combite phase and such transformation in the sodium calcium silicate system has no significant changes in the properties of Bioglass.[30]

FE-SEM and TEM micrographs in S2 clearly show the morphology and size of the n-BG particles, multilayers in rGO sheets and distribution of particles over the surface, edges and beneath the rGO sheets (S2 e) distribution indicated in different coloured dotted circles). Most particles of n-BG was observed to be between 50 nm – 70 nm in size and the morphology varied from spherical to irregular morphologies.

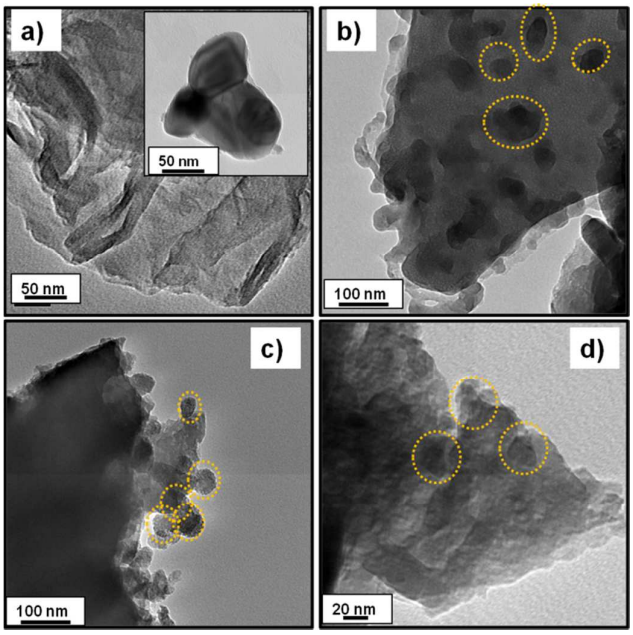

Fig.4 TEM micrographs of **a)** - rGO sheets, inset showing particles of n-BG, **b)** – Ultrasonicated, **c)** – Dispersion and **d)** – Simultaneous reduction. Dotted circles indicate the n-BG particles bonded to rGO sheets.

From HRTEM micrograph of Fig.4 a) above, shrinkage in rGO sheets is visualized and the inset image shows the particles of n-BG. In Fig.4 b), C) and d) summarises the n-BG particles bonded on the surface of the sheets, at the sides and beneath the layers of rGO sheets. In case of nanocomposites prepared by ultrasound and simultaneous reduction, the particles distribution over the sheets were uniform and number of particles bonded to sheets were higher than the dispersion method. More over in both the cases the particle size was observed to be smaller than that of dispersion method. The functionalization in the nanocomposites can be clearly understood from the Raman, FT-IR, XRD, FESEM and TEM data.

The optical data agrees with XRD pattern, FESEM and TEM images. From the above results, we could observe the integrity of n-BG particles and rGO sheets is not lost, except some changes in sodium calcium silicate phase which can be seen in XRD pattern. However, the change in size and morphology of the n-BG particles has changed in nanocomposites of ultrasonicated and simultaneously reduced samples which can be seen in FESEM and TEM images. The size of the n-BG particles has reduced considerably in ultrasonicated and simultaneously reduced samples when compared to dispersion samples.

Possible production of super-oxide anion radical can be studied using XTT dye (2, 3-bis (2-methoxy-4-nitro-5-sulfophenyl)-2H-tetrazolium-5-carboxanilide). The formation of super-oxide anion reduces the XTT dye molecules to water solvable formazan crystals, the absorbance of formazan could be read at 470 nm in UV-Visible spectroscopy. The intensity of formazan crystals produced directly implies the amount of super-oxide anion radicals produced. The procedure for this assay was followed as described by Shaobin Liu *et al* [31]

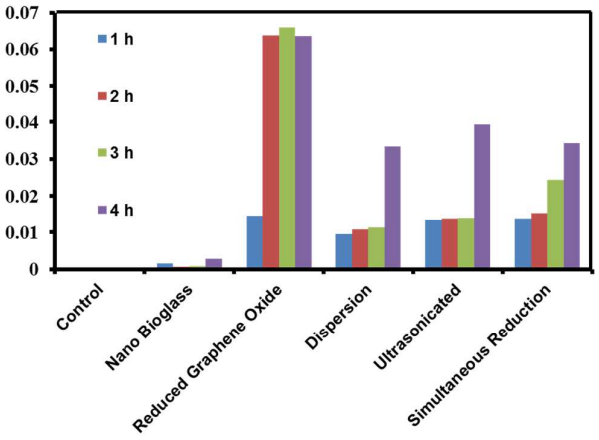

Fig.5 Super-oxide anion radical evaluation of n-BG particles, rGO sheets, nanocomposites prepared by dispersion, ultrasonication and simultaneous reduction using XTT dye.

In our study, 50 µg/ml of n-BG powders, rGO sheets and its nanocomposites were tested for $O_2^{\cdot-}$ production. The results plotted in fig. 5 shows the time dependent production of $O_2^{\cdot-}$ for all the samples up to 4 hours. From the results we could observe super-oxide anion production is very low in n-BG sample, and even at the fourth hour only traceable amount of super-oxide anion is observed. But rGO sheets sample showed the highest amount of $O_2^{\cdot-}$ production from the first hour till fourth hour. Nanocomposites fabricated by dispersion method at the given concentration produced considerable amount of super-oxide anion at the first hour and increased gradually with respect to time, but was lower than other two nanocomposites. In case of ultrasonicated and simultaneously reduced nanocomposites the production of super-oxide anion almost equal to rGO at the first hour readings, during the second and third hour reading the ultrasonicated nanocomposites did not show much increase in super-oxide anion production but there was steady increase in case of simultaneously reduced samples. At the fourth hour there was a sudden increase in super-oxide anion production in all nanocomposites with slight increased intensity in ultrasonicated samples. From the above results we could conclude n-BG as alone could not able to produce super-oxide anion, rGO sheets showed extensive production in super-oxide anion. Such phenomenon could be due to the interaction of XTT molecules with the high surface area in rGO sheets. In case of nanocomposites the production of super-oxide anion is lower than that of the rGO in all readings; this phenomenon could be due to the presence of SiO_2 in the composite. In work done by Zhang *et al* studies reveals that 100 µg/mL of graphene produces a lethal dose of ROS.[7] In our studies also it is observed rGO as alone produces more ROS than n-BG and its composites. Such phenomenon could be due to the interaction of rGO with n-BG. The diminution in size of n-BG particles in ultrasonicated and simultaneously reduced nanocomposites does not show any influence in the increment or decline in the production of $O_2^{\cdot-}$.From our observation we could understand that n-BG particles prepared by our method does not exhibit good $O_2^{\cdot-}$ production. Whereas rGO sheets produce high levels of $O_2^{\cdot-}$ which could be deleterious. The n-BG as alone is a good biocompatible material and rGO as alone is a good material for mechanical and biological properties. But by bringing together the properties of biocompatibility from n-BG and $O_2^{\cdot-}$ production of rGO to improve antibacterial activity, this materials could be a synergetic biomaterial for implant applications.

Conclusions

In conclusion n-BG powders are synthesised by sol-gel method, graphene oxide by modified Hummer's method and reduced using hydrazine hydrate. Successfully, three different strategies were employed to fabricate the nanocomposites using the n-BG, graphene oxide and rGO as raw materials. Due to the high surface activity of rGO sheets and n-BG particles were able to bond with the sheets surface in dispersion method. When nanocomposites were fabricated under ultrasound waves and simultaneous reduction of graphene oxide/n-BG complex the sodium ions in devitrite phase depleted leading to the domination of combite phase. Transformation and alterations in Si-O-Si bonds, crystallinity of n-BG were identified and studied using Raman, FT-IR spectroscopes and

XRD which are also in consistent with the FESEM and TEM micrographs, where the reduction in particle size and distribution of n-BG particles over the rGO sheets were clearly visualised. An attempt to understand the possible production of $O_2^{\cdot-}$ and their significance in killing the infectious agents was employed using XTT assay.

References

1 J.R. Jones, Acta Biomaterialia, 2013, **9**, 4457.
2 L. L. Hench, Biomed. Glasses, 2015, **1**, 1.
3 R. S. Pryce and L. L. Hench,J. Mater. Chem. , 2004, **14** , 2303.
4 M. Stevanović, N. Filipović, J. Djurdjević, M. Lukić, M. Milenković and A. Boccaccini, Colloildals and surfaces B: Biointerfaces, 2015, **132**, 208.
5 J. K. Leach, D. Kaigler, Z. Wang, P. H. Krebsbach and D. J. Mooney, Biomaterials, 2006, **27**, 3249.
6 K. Jurczyk, G. Adamek, M. M. Kubicka, J. Jakubowicz and M. Jurczyk, Materials, 2015, **8**, 1398.
7 Y. Zhang, S. F. Ali, E. Dervishi, Y. Xu, Z. Li, D. Casciano and A. S. Biris, ACS Nano, 2010, 4 (6), 3181.
8 T. R. Nayak, H. Andersen, V. S. Makam, C. Khaw, S. Bae, X. Xu, P. R. Ee, J. Ahn, B. H. Hong, G. Pastorin and B. Ozyilmaz, ACS Nano, 2011, 5 (6), 4670.
9 H. Porwal, S. Grasso, L. C. Arias, C. Li, A.R. Boccaccini, M. J. Reece, J Mater Sci: Mater Med, 2015, **25**, 1403.
10 C. Gao, T. Liu, C. Shuai and S. Peng, Sci Rep, 2014, 16;4:4712.
11 H. Pan, X. Xu and R. Tang, RSC Adv, 2014, 4, 25398.
12 H. Liu, P. Xi, G. Xie, Y. Shi, F. Hou, L. Huang, F. Chen, Z. Zeng, C. Shao and J. Wang, J. Phys. chem. C, 2012, 116 (5), 3334.
13 G. Bharath, R. Madhu, S. Chen, V. Veeramani, A. Balamurugan, D. Mangalaraj, C. Viswanathan and N. Ponpandian, J. Mater. Chem. B, 2015, 3, 1360.
14 M. J. Fernández-Merino, L. Guardia, J. I. Paredes, S. Villar-Rodil, P. Solís-Fernández, A. Martínez-Alonso and J. M. D. Tascón, *J. Phys. Chem. C*, 2010, 114 (14), 6426.
15 D. Konios, C.Petridis, G. Kakavelakis, M. Sygletou, K. Savva,E. Stratakis and E. Kymakis, Adv Funct Mater., 2015; 25 (15): 2213.
16 D. R. Dreyer, S. Park, C. W. Bielawski and R. S. Ruoff, Chem. Soc. Rev., 2010, 39, 228.
17 D. Mohan, S.K. Misra,T. J. Brunner, A.R. Boccaccini, W.J. Stark, European Cells and Materials, Vol. 16, Suppl. 1, 8
18 W.Y. Gong, Y. M. Dong, X. F. Chen, B. Karabucak, CJDR, 2012; 15 (2), 145.
19 D. Durgalakshmi, S. Balakumar, C.A. Raja, R. P. George and U.K. Mudali, J. NanosciNanotechnol., 2015, 15, (6), 4285.
20 D. C. Marcano, D.V. Kosynkin, J. M. Berlin, A. Siniskii, Z. Sun, A. Slesarev, L. B. Alemany, W. Lu and J. M. Tour, ACS Nano, 2010, 24, 4 (8), 4806.
21 S. Stankovich, D. A. Dikin, R. D. Piner, K. A. Kohlhaas, A. Kleinhammes, Y. Jia, Y. Wu, S. T. Nguyen and R. S. Ruoff, Carbon, 2007, 45 (7), 1558.
22 L. Marsich, L. Moimas, V. Sergo and C. Schmid, Spectroscopy, 2009, 23 (3-4), 227.
23 Y. Miroshnikov, G. Grinbom, G. Gershinsky, G. D. Nessim and D. Zitoun, Faraday Discuss., 2014, 173, 391.
24 N. Wu, X. She, D. Yang, X. Wu, F. Su and Y. Chen, J. Mater. Chem., 2012, 22, 17254.
25 E. R. Essien, L. A. Adams, R. O. shaibu, A. Oki, J. Biomedical Science and Engineering, 2013, 6, 258.
26 A. R. Boccaccini, Q. Chen, L. Lefebvre, L. Gremillard and J. Chevalier, Faraday Discuss, 2007, 136 (27), 107.
27 I. Battisha and A. E. Nahrawy, NJGC, 2012, 2 (1), 17.
28 S. M. Salman, S. N. Salama and H. A. Abo-Mosallam, Ceramic International, 2012, 38 (1), 55.
29 C. Volzoneand F. M. Stábile, New Journal of Glass and Ceramics, 2013, 3, 53.
30 M. N. Rahaman, D. E. Day, B. S. Bal, Q. Fu, S. B. Jung, L. F. Bonewald and A. P. Tomsia, ActaBiomater, 2011, 7 (6), 2355.
31 S. Liu, T. H. Zeng, M. Hofmann, E. Burcombe, J. Wei, R. Jiang, J. Kong and Y. Chen, ACS Nano, 2011, 5 (9), 6971.